

PACS numbers: 42.55.Rz; 42.55.Xi; 42.60.Jf
DOI: 10.1070/QE2015v045n06ABEH015287

Optimisation of the parameters of a pump chamber for solid-state lasers with diode pumping by the optical boiler method

V.V. Kiyko, V.I. Kislov, E.N. Ofitserov, A.G. Suzdal'tsev

Abstract. **A pump chamber of the optical boiler type for solid-state lasers with transverse laser diode pumping is studied theoretically and experimentally. The pump chamber parameters are optimised using the geometrical optics approximation for the pump radiation. According to calculations, the integral absorption coefficient of the active element at a wavelength of 808 nm is 0.75–0.8 and the relative inhomogeneity of the pump radiation distribution over the active element volume is 17%–19%. The developed pump chamber was used in a Nd:YAG laser. The maximum cw output power at a wavelength of 1064 nm was ~480 W at the optical efficiency up to 19.6%, which agrees with theoretical estimates.**

Keywords: *solid-state laser, pump chamber, laser diode arrays, optimisation model.*

1. Introduction

At present, much attention is paid to the study and development of high-power (up to 1 kW) solid-state lasers (SSLs) with laser diode (LD) pumping (see [1, 2] and referenced therein). These lasers have the following advantages over the lasers of other types: high optical efficiency (10%–20%), controllable temperature distribution in the active element (AE) volume, and high operational lifetime (~10000 h).

The efficiency of SSLs depends to a large extent on the pump chamber configuration. The optimisation parameters of lamp-pumped SSLs are the positions of light sources, the geometry and optical characteristics of reflectors, and the conditions of interaction of the laser radiation with the plasma of pump sources [3, 4]. For these pump chambers, there exists a mathematical tool (see [3] and references therein), which takes into account multiple passes of the optical system and allows one to perform engineering calculation of pump chambers with both mirror and diffuse reflectors.

Of great practical interest for LD-pumped lasers are cylindrical pump chambers in the form of a closed optical chain of the optical boiler type [3–5] with transverse pumping by several LD arrays oriented along the AE optical axis. In this case, the pump radiation returns to the AE and is absorbed in it in the process of multiple passes inside the pump chamber. The directional diagram of LD radiation has a width of ~30°, which makes it possible to create compact and highly efficient pump chambers without additional devices for matching the beam paths with the AE geometry. These pump chambers are multipass, multilayer, and quasi-symmetric (in design) systems, in which optimisation must be performed with respect to the radius, thickness, and refractive index of the reflector; to the thickness and refractive index of the cooling medium; and to the AE diameter.

The results of investigations of lamp-pumped SSLs cannot be directly used for the development of pump chambers for LD-pumped SSLs because they do not take into account the specific features of radiation of LD arrays, as well as the fact that the optical boiler system is multilayer. A pump-chamber beam model taking into account that an LD pump system is multilayer is presented in [5], but the necessity of taking into account multiple passes in the optical system creates some calculation problems.

In the present work, we propose a semi-analytical optimisation model of a cylindrical optical boiler, which is developed in the geometrical optics approximation (ray approximation) and takes into account the above-mentioned specific features of SSLs with diode arrays. As the main pump chamber characteristic, we take the integral absorption coefficient (IAC), i.e., the fraction of LD radiation absorbed in the AE. The parameter optimisation results, as well as the results of experimental investigations of a SSL pump chamber with five LD arrays, are discussed.

2. Pump chamber optimisation model

Figure 1 presents the schemes of a pump chamber cross section and beam paths between layers with different refractive indices. The pump LD radiation (Fig. 1a) enters the pump chamber through antireflection-coated (for the pump wavelength) slits and is partially absorbed in the AE after multiple reflections from the inner surface of the reflector.

The IAC was calculated in the geometrical optics approximation. It was assumed that the intensity distribution is steady-state in the transverse cross section, which is perpendicular to the cylindrical AE axis, and does not depend on the cross section position along the optical axis of the system. In the model, we assumed that the intensities of beams coupled into the pump chamber with identical angles of reflection from the reflector undergo identical relative changes upon propagation. The beam propagation trajectory is a zigzag line, whose characteristics were calculated using Snell's law [6]. The refracting surfaces (see Fig. 1b) are numbered from

V.V. Kiyko A.M. Prokhorov General Physics Institute, Russian Academy of Sciences, ul. Vavilova 38, 119991 Moscow, Russia; ITMO University, Kronverkskii prosp. 49, 197101 St. Petersburg, Russia; e-mail: hkww@mail.ru;
V.I. Kislov, E.N. Ofitserov, A.G. Suzdal'tsev A.M. Prokhorov General Physics Institute, Russian Academy of Sciences, ul. Vavilova 38, 119991 Moscow, Russia; e-mail: oficerov@ran.gpi.ru

Received 22 July 2013; revision received 24 November 2014
Kvantovaya Elektronika **45** (6) 511–514 (2015)
Translated by M.N. Basieva

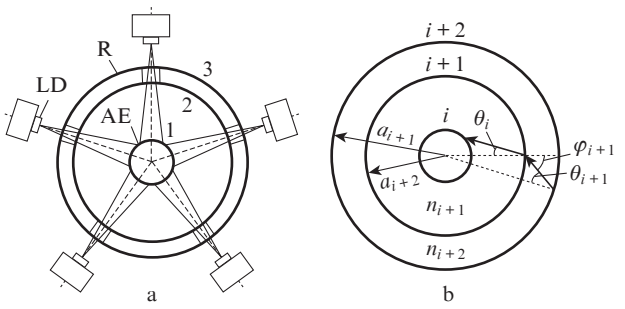

Figure 1. (a) Pump chamber scheme: (LD) laser diode array; (AE) active element; (R) reflector; (1)–(3) surfaces. (b) Schematic of beam paths in the pump chamber cross section.

the centre ($i = 1$) to the periphery ($i = N - 1$), the reflecting surface of the reflector having the number $i = N$.

First, we find the intensity reflection coefficient for the AE. Taking into account multiple beam paths inside the AE, this coefficient is

$$\rho_1(\theta_1) = \begin{cases} R_1(\varphi_1) + T_1(\varphi_1)^2 \exp(-\sigma l)/[1 - R_1(\varphi_1)\exp(-\sigma l)], \\ 1, \text{ if } |\sin\theta_1| > \min(n_2 a_1/(n_1 a_2); a_1/a_2), \end{cases} \quad (1)$$

where θ_1 is the angle between a beam directed to the AE and the AE diameter drawn through the point of intersection of this beam with surface 2; R_1 and T_1 are the Fresnel power reflection and transmission coefficients dependent on the angle of incidence φ_1 [6] for surface 1; n_1 and n_2 are the refractive indices of the AE and the medium between surfaces 1 and 2; $l = 2a_1\cos\theta_0$ is the beam path length in the AE [$\sin\theta_0 = (n_2 a_2/n_1 a_1)\sin\theta_1$, $\sin\varphi_1 = (a_2/a_1)\sin\theta_1$]; σ is the AE absorption coefficient per unit length; and a_1 and a_2 are the radii of the AE and surface 2. According to (1), the reflection coefficients of beams missing the AE were taken to be $\rho_1 = 1$.

Then, we introduce into consideration the power reflection coefficients ρ_i and ρ_{i+1} for cylindrical systems confined by surfaces i and $i + 1$, respectively. Let us write ρ_{i+1} via ρ_i considering the cylindrical layer between surfaces $i + 1$ and i as a multipass system. The system was analysed based on the same considerations as those used when investigating a multipass Fabry–Perot interferometer [6, 7]. As a result, we have

$$\rho_{i+1} = \begin{cases} R_{i+1} + \rho_i T_{i+1}^2/(1 - \rho_i R_{i+1}), \\ 1, \text{ if } |\sin\theta_{i+1}| > \min(n_{i+2} a_{i+1}/(n_{i+1} a_{i+2}), a_{i+1}/a_{i+2}), \end{cases} \quad (2)$$

where $\rho_{i+1} = \rho_{i+1}(\theta_{i+1})$; $\rho_i = \rho_i(\theta_i)$; and $R_{i+1} = R_{i+1}(\varphi_{i+1})$ and $T_{i+1} = T_{i+1}(\varphi_{i+1})$ are the Fresnel power reflection and transmission coefficients for surface $i + 1$. The symbols in (2) are clear from Fig. 1: θ_i and θ_{i+1} are the refraction angles for surfaces $i + 1$ and $i + 2$, respectively; φ_{i+1} is the angle of incidence on surface $i + 1$; n_{i+1} is the refractive index of the layer between surfaces i and $i + 1$ (refractive index n_{i+2} belongs to the layer between surfaces $i + 1$ and $i + 2$); and a_{i+1} and a_{i+2} are the radii of surfaces $i + 1$ and $i + 2$, respectively. In this case,

$$\sin\theta_{i+1} = \frac{n_{i+1} a_{i+1}}{n_{i+2} a_{i+2}} \sin\theta_i, \quad \sin\varphi_{i+1} \frac{n_{i+1}}{n_{i+2}} \sin\theta_i.$$

Relations (1) and (2) form a recurrent system and allow one to determine the reflection coefficient of the entire system inside the outer surface of the reflector. Introducing into consideration the transmission coefficient $\tau_k = 1 - \rho_k$ ($k = 1, N - 1$), we find from relation (2) by algebraic manipulations the formula

$$\tau_{N-1}(\theta_{N-1}) = \frac{\tau_1(\theta_1)}{1 + \tau_1(\theta_1) \sum_2^{N-1} R_k(\varphi_k)/T_k(\varphi_k)}. \quad (3)$$

From (3), it follows that the smaller the number of layers and the closer their refractive indices, the higher the AE absorption.

Then, we considered the following balance equations for the intensities of beams inside the layer confined by the reflector and surface $N - 1$:

$$V = [P_\mu f(\theta) + P g(\theta)]\rho_{N-1}(\theta), \quad (4)$$

$$P_V = P_\mu \int \rho_{N-1} f(\theta)\,d\theta + P \int \rho_{N-1} g(\theta)\,d\theta, \quad (5)$$

$$\mu P_V = P_\mu, \quad (6)$$

where P is the diode array power coupled into the system; P_μ is the radiation power reflected by the reflector; V is the intensity of the beam incident on the reflector; $P_V = \int V d\theta$ is the radiation power incident on the reflector; $\rho_{N-1} = 1 - \tau_{N-1}$; $\theta = \theta_{N-1}$; $f(\theta)$ is the scattering diagram for the outer surface of the reflector; μ is the power reflection coefficient of the reflector; and $g(\theta)$ is the angular distribution of the diode array radiation. Equations (4) and (6) describe the intensity and power of radiation propagating toward the reflector, while Eqn (5) describes the power reflected by the reflector. Thus, based on (4)–(6), we can calculate the total radiation intensity coupled into the system by the formula

$$V_\Sigma = P_\mu f(\theta) + P g(\theta) = P\left(\frac{\mu f(\theta)\int \rho_{N-1} g\,d\theta}{1 - \mu\int \rho_{N-1} g\,d\theta} + g(\theta)\right), \quad (7)$$

the power absorbed in the AE being

$$Q = \int V_\Sigma (1 - \rho_{N-1})\,d\theta. \quad (8)$$

Taking into account (7) and (8), the IAC of the pump chamber is determined as

$$\eta = s\left(\frac{1 - (1 - \mu)\int \rho_{N-1} g\,d\theta}{1 - \mu\int \rho_{N-1} f\,d\theta}\right), \quad (9)$$

where the coefficient s takes into account partial screening of LD radiation by the input slit. In addition, part of radiation leaves the system via the entrance apertures. The fraction of radiation power left in the system is estimated as

$$\xi = 1 - N_L S/(2\pi a_N), \quad (10)$$

where N_L is the number of diode arrays, S is the entrance hole width, and a_N is the reflector radius. The loss factor (10) is taken into account in (9) by replacing μ with $\mu\xi$.

The obtained relations can be extended to a two-dimensional model. In this case, the beam trajectory is described by two angular coordinates. Therefore, the Fresnel coefficients become functions of two variables, and the integration in the final relations is performed over both of them.

The reflection coefficients also depend on the radiation polarisation, which is close to *S*-oriented for LDs [1, 5] and almost absent for the radiation scattered by the reflector. Correspondingly, the function ρ_{N-1} in (9) is determined for the *S*-polarised radiation in the numerator and as an average for two polarisations in the denominator.

3. Calculation results

Based on (9), we performed optimisation calculations of the main parameters of the pump chamber whose scheme is shown in Fig. 1a. In this case, the system has three interfaces ($N = 3$). The angular distribution $g(\theta)$ of radiation of LD arrays was taken to be Gaussian, the scattering diagram $f(\theta)$ for the outer mirror reflector corresponded to the Lambert law, and the reflection coefficient of this reflector was 0.98. In Fig. 1a, the medium between surfaces 3 and 2 is quartz (refractive index $n_3 = 1.5$). The space between cylindrical surfaces 2 and 1 is filled by cooling water ($n_2 = 1.33$) flowing along the Nd:YAG AE ($n_1 = 1.82$). The cylindrical AE is 6.3 mm in diameter and 130 mm long. The chamber with a length of 530 mm is formed by two plane mirrors with reflection coefficients 99% and 64%. The number of LD arrays is five, the pump wavelength is $\lambda = 808 \pm 2$ nm, and the Nd concentration in the crystal is 0.8%–0.9%. The AE absorption coefficient at the pump wavelength is $\sigma = 0.3$ mm^{-1}. These parameters were chosen with regard to the technical and technological limitations. We optimised the reflector diameter and reflection coefficient, the size of the slit (entrance aperture for pump radiation), and the thickness of the quartz layer of the reflector.

Some results of the calculations of the pump chamber characteristics are presented in Figs 2a–2c. From Fig. 2a, one can see that, with increasing reflector radius a_3, the IAC decreases due to an increasing number of beams missing the AE.

Analysis of Fig 2b reveals that there exits an optimal slit width ($S \approx 1.5$–2.5 mm). The existence of an extremum is explained by the competition of two factors: on the one hand, a decrease in the slit size leads to a decrease in the IAC due to confinement of the pump beam by the slit aperture, and, on the other hand, an increase in the slit width increases the fraction of radiation power that leaves the chamber through these slits instead of reflecting from the reflector surface.

Figure 2c shows the dependence of the IAC on the reflection coefficient μ. With increasing μ, radiation power inside the pump chamber and, hence, the IAC increase. Within the presented pump chamber optimisation model, we estimated the inhomogeneity of the pump radiation distribution over the AE volume (Fig. 2d). The homogeneity of filling of the AE volume by the pump radiation was estimated as the root-mean-square deviation δ of radiation intensity from average. An increase in the reflector radius increases the fraction of radiation scattered by the reflector, and, therefore, improves

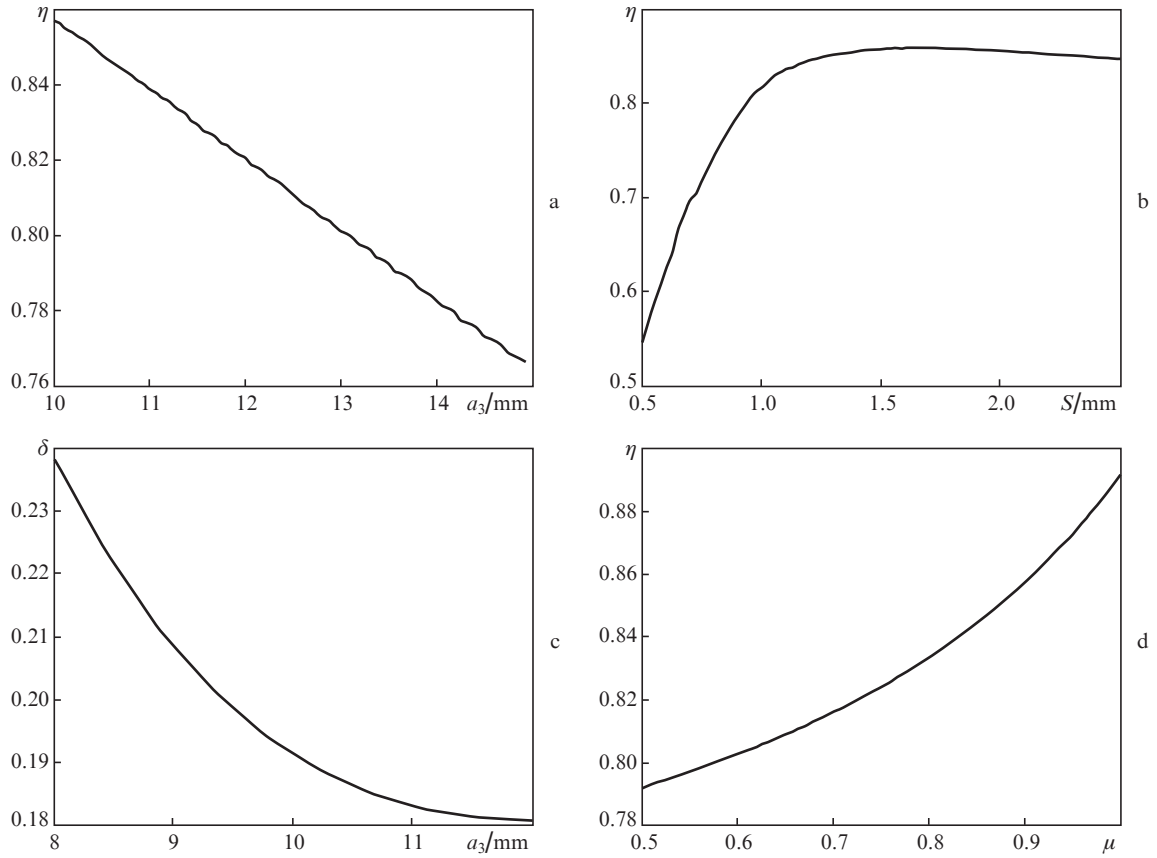

Figure 2. Dependences of the IAC on (a) the reflector radius a_3 ($\mu = 0.9$, AE diameter $a_1 = 6$ mm, AE linear absorption coefficient $\sigma = 0.4$ mm^{-1}, AE length $L = 120$ mm), (b) the entrance aperture width S ($\mu = 0.9$, $2a_3 = 20$ mm) and (c) the reflector reflection coefficient μ ($S = 2$ mm, $2a_3 = 20$ mm), as well as (d) dependence of the intensity root-mean-square deviation from average δ on a_3 ($\mu = 0.9$, $a_1 = 6$ mm, $\sigma = 0.4$ mm^{-1}, $L = 120$ mm, $S = 2.5$ mm).

the homogeneity of pump radiation distribution inside the pump chamber.

4. Experimental results

Using the presented results, we developed a pump chamber (Fig. 3) for transversely diode-pumped solid-state lasers. The technical characteristics of the pump chamber are partially presented in the previous section; the optimised slit width and reflector diameter were 2.5 mm and 21 mm, respectively. The total pump power reached 2.5 kW.

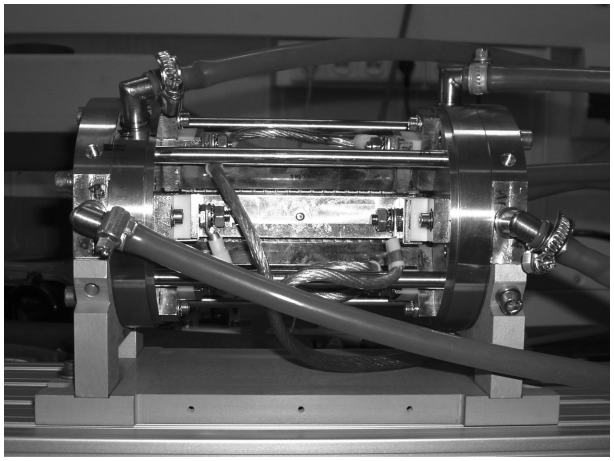

Figure 3. Pump chamber photograph.

We preliminary tested the laser setup. Figure 4 shows the dependences of the output power and the M^2 parameter on the pump power. The maximum laser power (at 1064 nm) was 480 W. The optical-to-optical laser efficiency reached 19.6%. In experiments with an AE with a ground side surface, the laser power was almost the same. According to theoretical estimates, the optical-to-optical laser efficiency η_{las} is equal to the product of three components [8], i.e., $\eta_{las} = \eta_S \eta \eta_r$, where η_S is the coefficient taking into account the Stokes losses ($\eta_S \approx 0.76$); η is determined by formula (9) ($\eta = 0.75-0.8$); and $\eta_r = (1 - P_{th}/P)\{1/[1 + 2\sigma L_r/\ln(1/R)]\}$ is the resonator efficiency ($\eta_r \approx 0.45$), where P_{th} is the threshold pump power, P is the pump power coupled into the chamber, σ corresponds to the dissipative losses in the chamber, L_r is the resonator length, and R is the reflection coefficient of the output mirror. In our case, the calculated optical-to-optical efficiency is 25%–27%, which is somewhat higher than the experimental value. The relative homogeneity corresponded to $\delta \approx 17.19\%$.

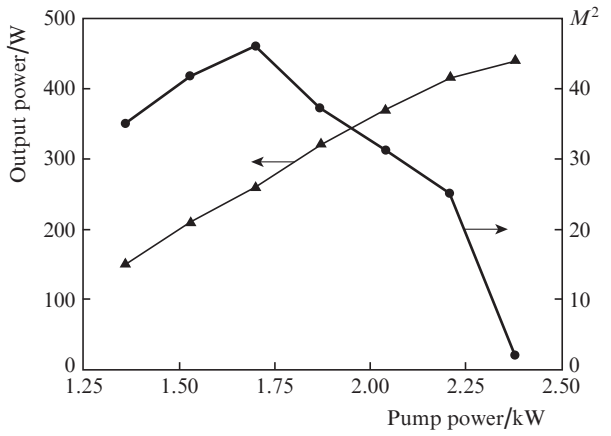

Figure 4. Dependences of the output laser power and the M^2 parameter on the pump power.

An increase in the pump power enhances the thermal lens effect. When the pump power exceeds 2 kW, the laser chamber configuration, with allowance for the thermal lens, becomes slightly unstable, while the quality parameter M^2 and, hence, divergence of the laser beam decrease. At the highest pump levels, the laser beam quality approaches the diffraction limit. This testifies to the dominance of the spherical component in the thermal lens.

5. Conclusions

A semi-analytical optimisation model of a pump chamber of the optical boiler type is developed. The theoretical calculations are performed in the geometrical optics approximation taking into account that optical boiler is a multipass system. Optimisation calculations are performed for a pump chamber with transverse pumping of the AE by five laser diode arrays. The calculated integral absorption coefficient of a Nd:YAG AE at a pump wavelength of 808 nm is 0.75–0.8, and the relative pump radiation inhomogeneity over the AE volume is 17%–19%.

The maximum experimental cw output power ($\lambda = 1064$ nm) of a laser with the developed pump chamber was ~480 W at $M^2 \approx 2.1$ and an optical-to-optical efficiency of ~19.6%. The laser beam quality approaches the diffraction limit at the highest pump levels.

In future calculations of pump chambers, it seems reasonable to take into account the amplified spontaneous emission, which, in the steady-state lasing regime, is confined inside the pump chamber and decreases the laser efficiency. In addition, it is interesting to study the thermal lens formed in the AE during pumping and lasing.

Acknowledgements. This work was partially supported by the Russian Foundation for Basic Research (Grant No. 13-02-00942).

References

1. Grechin S.G., Nikolaev P.P. *Kvantovaya Elektron.*, **39** (1), 1 (2009) [*Quantum Electron.*, **39** (1), 1 (2009)].
2. Borisov B.N., Demkin V.K., et al. http://vk.cc/3OueGP.
3. Stepanov B.I. *Metody rascheta opticheskikh kvantovykh generatorov* (Methods of Calculating Optical Quantum Generators) (Minsk: Nauka i Tekhnika, 1968) Vol. 2.
4. Basov N.G., Gerasimov V.A., Gradov V.M., et al. Preprint FIAN, No. 106 (Moscow, 1984).
5. Wang Y., Kan H. *Opt. Commun.*, **226**, 303 (2003); *Opt. Lasers Eng.*, **45**, 93 (2007).
6. Born M., Wolf E. *Principles of Optics* (Pergamon Press, New York, 1964).
7. Kiyko V.V., Kislov V.I., Ofitserov E.N. *Kvantovaya Elektron.*, **40** (6), 556 (2010) [*Quantum Electron.*, **40** (6), 556 (2010)].
8. Zverev G.M., Golyaev Yu.D., Shalaev E.A., Shokin A.A. *Lazery na alyumoittrievom granate s neodimom* (Neodymium-Doped Yttrium–Aluminium–Garnet Lasers) (Moscow: Radio i Svyaz', 1985).